ARL-TR-8875 ● DEC 2019

A 2-D Lookup Table for Monopulse Radar

by Michael L Don

NOTICES

Disclaimers

The findings in this report are not to be construed as an official Department of the Army position unless so designated by other authorized documents.

Citation of manufacturer’s or trade names does not constitute an official endorsement or approval of the use thereof.

Destroy this report when it is no longer needed. Do not return it to the originator.

ARL-TR-8875 ● DEC 2019

A 2-D Lookup Table for Monopulse Radar

Michael L Don
Weapons and Materials Research Directorate, CCDC Army Research Laboratory

REPORT DOCUMENTATION PAGE	*Form Approved* *OMB No. 0704-0188*

1. REPORT DATE *(DD-MM-YYYY)*	**2. REPORT TYPE**	**3. DATES COVERED (From - To)**
December 2019	Technical Report	July–September 2019

4. TITLE AND SUBTITLE
A 2-D Lookup Table for Monopulse Radar

5a. CONTRACT NUMBER

5b. GRANT NUMBER

5c. PROGRAM ELEMENT NUMBER

6. AUTHOR(S)
Michael L Don

5d. PROJECT NUMBER

5e. TASK NUMBER

5f. WORK UNIT NUMBER

7. PERFORMING ORGANIZATION NAME(S) AND ADDRESS(ES)
Director
CCDC Army Research Laboratory
ATTN: FCDD-RLW-LF
Aberdeen Proving Ground, MD 21005-5069

8. PERFORMING ORGANIZATION REPORT NUMBER
ARL-TR-8875

9. SPONSORING/MONITORING AGENCY NAME(S) AND ADDRESS(ES)

10. SPONSOR/MONITOR'S ACRONYM(S)

11. SPONSOR/MONITOR'S REPORT NUMBER(S)

12. DISTRIBUTION/AVAILABILITY STATEMENT
Approved for public release; distribution is unlimited.

13. SUPPLEMENTARY NOTES
ORCID ID: Michael L Don, 0000-0003-8021-9066

14. ABSTRACT
This report details the construction of a 2-D lookup table for monopulse radar. Linear models and 1-D lookup tables fail to capture the change of the monopulse ratios over their whole 2-D surfaces. 2-D lookup tables capture this effect, resulting in higher performance. The 2-D lookup table is evaluated with both a Gaussian antenna model and an alternative antenna model. Details such as the range of ϕ and θ used to evaluate the table, the table resolution, and the method used to resolve missing or multiple points all affect the overall performance. Finally, noise and detection models are added, allowing for the optimization of system parameters through trade studies.

15. SUBJECT TERMS
radar, monopulse, inverse problem, antenna modeling, direction of arrival

16. SECURITY CLASSIFICATION OF:			**17. LIMITATION OF ABSTRACT**	**18. NUMBER OF PAGES**	**19a. NAME OF RESPONSIBLE PERSON**
					Michael L Don
a. REPORT	**b. ABSTRACT**	**c. THIS PAGE**			**19b. TELEPHONE NUMBER (Include area code)**
Unclassified	Unclassified	Unclassified	UU	33	410-306-0775

Standard Form 298 (Rev. 8/98)
Prescribed by ANSI Std. Z39.18

Contents

List of Figures

List of Tables

Acknowledgments

The author would like to acknowledge Mark Govoni for introducing me to monopulse radar, and for instigating this research.

1. Introduction

Monopulse radar, as the name implies, uses multiple antennas to determine the direction of arrival (DOA) of a single radio pulse. This is in contradistinction to other radar techniques, such as scanning radars, that require multiple measurements to determine DOA. Traditionally, monopulse radars have processed their antenna outputs using analog circuits. This limits the scope of processing algorithms to those that can easily be implemented as analog circuits. Digital processing of monopulse radar allows for the implementation of a broader range of algorithms. This report investigates one such algorithm, the interpolation of a 2-D lookup table for monopulse signal processing.

Monopulse radar dates back to 1944[1] and is the most common type of radar is use today. Monopulse applications include the following[2]:

- Control of gunfire and missile launch and guidance
- Tracking both friendly or hostile objects at long range by land, sea, air, or space
- Intelligence on the trajectory, size, shape, and rotation of objects at long distance
- Instrumentation radar for tracking during testing or exercises

Monopulse radar processing uses phase, amplitude, or both phase and amplitude information from the antenna array. There are many ways to process this information. Most literature addresses theoretical models that do not assume the existence of experimental calibration data that naturally leads to a lookup table implementation. Literature that does mention the use of lookup tables[3,4] do not provide specific details about table construction. This report investigates the problems associated with the design of a lookup table for 4-element amplitude-omparison monopulse radar. Additionally, a monopulse radar model is developed that can be used for system simulation and trade studies.

The report is organized as follows. First, a simple monopulse radar model using a Gaussian antenna pattern is presented. Next, the performance of a linear processing model and a 1-D lookup table are evaluated. Then a 2-D table is constructed and compared with the 1-D processing models. This table is used, together with the addition of a noise model, to conduct an example system trade study. An alternative antenna model is evaluated leading to modifications in the table construction. Finally, RF detection circuitry is added as the last piece of the system model.

2. Monopulse Radar Model

A monopulse antenna array with four elements is shown in Fig. 1.

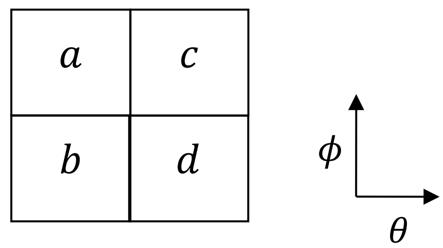

Fig. 1 Four-element monopulse radar diagram

The antenna output amplitudes, a, b, c, and d, can be simulated using an Gaussian antenna model[5]:

$$E(\theta, \phi) = e^{\frac{-(\theta-\delta_\theta)^2-(\phi-\delta_\phi)^2}{K}}, \tag{1}$$

where δ_θ and δ_ϕ are pattern offsets and constant K scales the beamwidth. Figure 2 shows antenna patterns for $K = 0.5$ and values of δ_θ and δ_ϕ defined in Table 1.

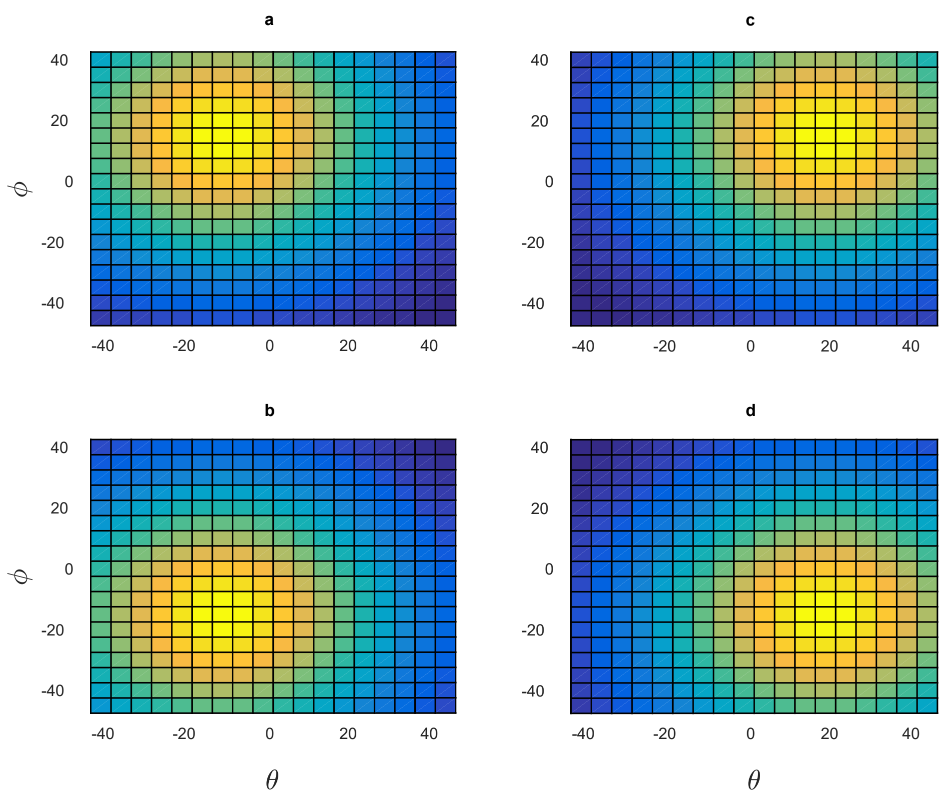

Fig. 2 Gaussian antenna patterns for the four monopulse elements

Table 1 Pattern offsets used in Fig. 1

Element	$\boldsymbol{\delta_\theta}$	$\boldsymbol{\delta_\phi}$
a	–15°	15°
b	–15°	–15°
c	15°	15°
d	15°	–15°

Given the measured antenna element amplitudes for a given θ and ϕ, the following values are defined[6]:

$$\Delta_\theta = (c + d) - (a + b). \tag{2}$$

$$\Delta_\phi = (a + c) - (b + d). \tag{3}$$

$$\Sigma = a + b + c + d. \tag{4}$$

$$r_\theta = \Delta_\theta / \Sigma. \tag{5}$$

$$r_\phi = \Delta_\phi / \Sigma. \tag{6}$$

r_θ and r_ϕ are the monopulse ratios in azimuth and elevation, respectively, and are used to create gain independent inverse models. Plots of r_θ and r_ϕ are shown in Fig. 3 for θ and ϕ in the interval [45°,45°]. The bottom plots are side views of the top plots, displaying r_θ and r_ϕ across a single angle.

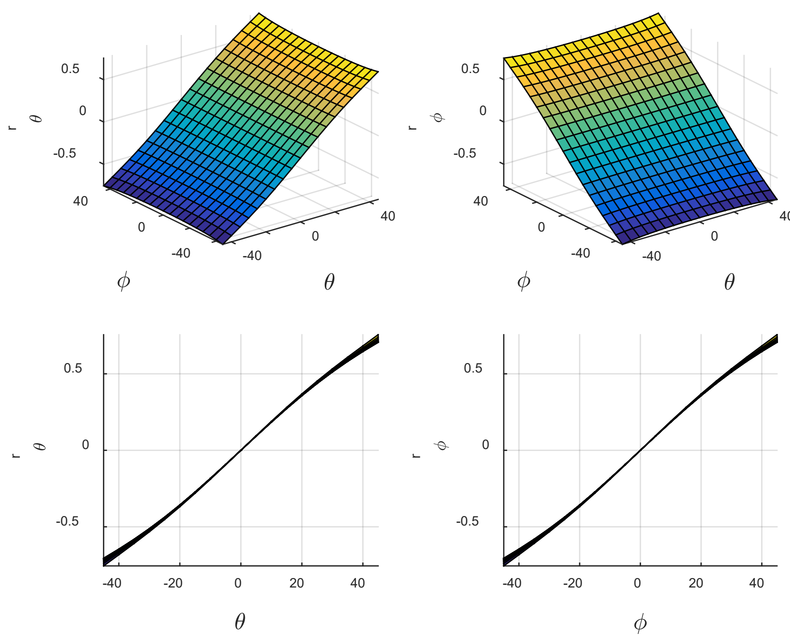

Fig. 3 $\boldsymbol{r_\theta}$ and $\boldsymbol{r_\phi}$ surfaces over the interval [45°,45°] for $\boldsymbol{\theta}$ and $\boldsymbol{\phi}$ (top), and side views showing $\boldsymbol{r_\theta}$ vs. $\boldsymbol{\theta}$ and $\boldsymbol{r_\phi}$ vs. $\boldsymbol{\phi}$ (bottom)

3. 1-D Models

3.1 Linear Model

Observe that r_θ and r_ϕ in Fig. 3 are fairly linear across θ and ϕ, respectively. This allows for accurate linear models

$$r_\theta = m_\theta \tag{7}$$

and

$$r_\phi = m_\phi \phi \ , \tag{8}$$

which are easily inverted to determine θ and ϕ given r_θ and r_ϕ. To determine the values of m_θ and m_ϕ, the r_θ and r_ϕ surfaces are averaged across ϕ and θ, respectively. The top two plots of Fig. 4 show these average r_θ and r_ϕ curves, while the bottom two plots show their actual slopes.

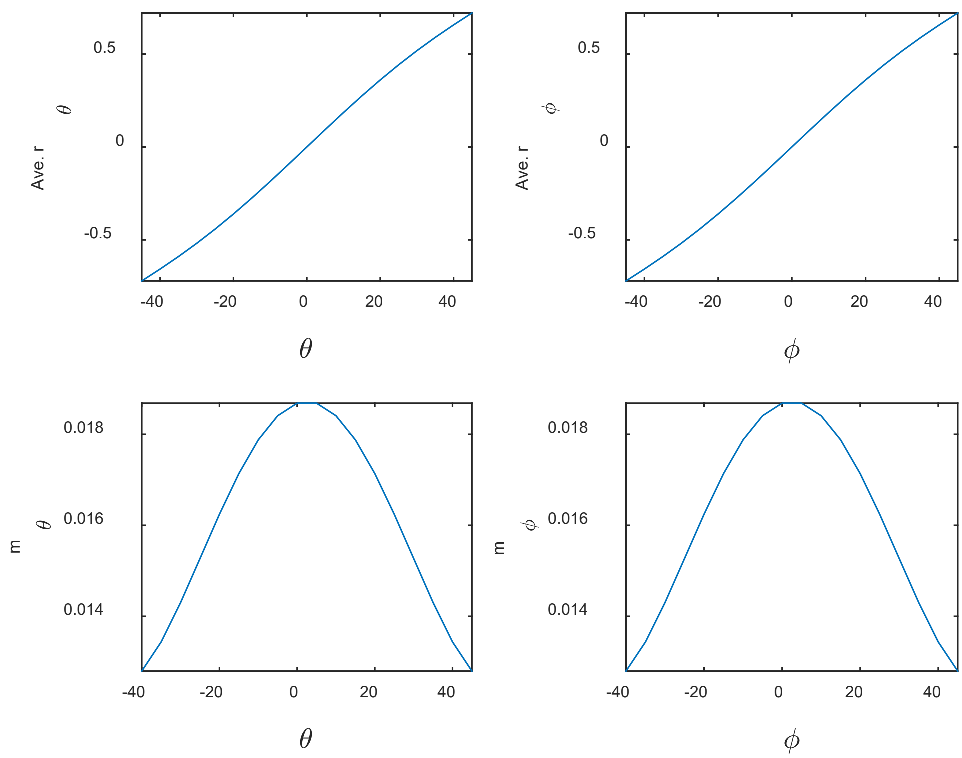

Fig. 4 (top) r_θ and r_ϕ averaged across ϕ and θ, respectively, and (bottom) the slopes of these average curves m_θ and m_ϕ

The best least-squares linear fit to the average r_θ and r_ϕ curves is used to determine scalar values of m_θ and m_ϕ in Eqs. 7 and 8. The error using these linear models to find θ and ϕ given r_θ and r_ϕ is shown in Fig. 5.

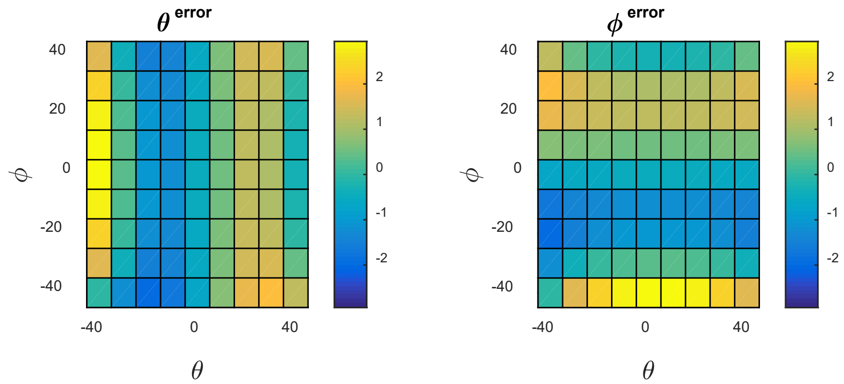

Fig. 5 Error using an inverse linear model to determine θ and ϕ given r_θ and r_ϕ

3.2 1-D Lookup Table

Instead of a linear model, the average r_θ and r_ϕ curves can be recorded in a lookup table and interpolated to determine θ and ϕ. The plots in Fig. 6 show the results of this method using a lookup table with 5° resolution. In this case, the error distribution is different than the linear model but the maximum error is about the same. Even though the 1-D model fits the average r_θ and r_ϕ curves better than the linear model, it still ignores the change in r_θ and r_ϕ along ϕ and θ, respectively.

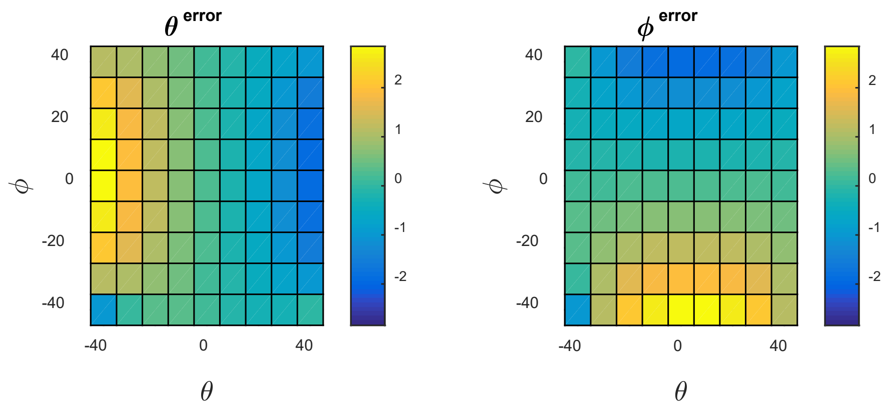

Fig. 6 Error using a 1-D lookup table to determine θ and ϕ given r_θ and r_ϕ

4. 2-D Lookup Table

4.1 Lookup Table Construction

To capture the change in r_θ and r_ϕ along ϕ and θ, the entire r_θ and r_ϕ surfaces can be used to create a 2-D lookup table. Each value of r_θ defines a curve in θ across ϕ. Similarly, r_ϕ defines a curve in ϕ across θ. The intersection of these curves gives the (θ, ϕ) point that maps to (r_θ, r_ϕ). Figure 7 shows these curves for $r_\theta = 0.59$ and $r_\phi = 0.50$.

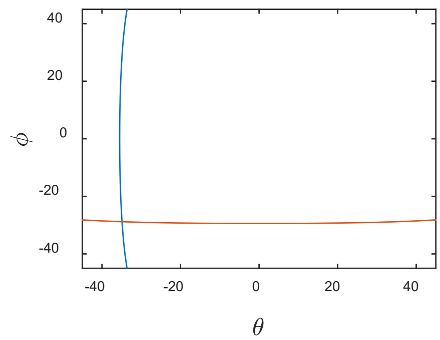

Fig. 7 Example curve in θ across ϕ for (blue) $r_\theta = 0.59$ and (red) curve in ϕ across θ for $r_\phi = 0.50$. The intersection point maps (r_θ, r_ϕ) to (θ, ϕ).

Figures 8 and 9 show the results of using this method to fill in 2-D lookup tables for θ and ϕ. Cases where r curves have no intersections or multiple intersections are excluded from the plots. Of course, given a table of infinite resolution and maximum range, the angles can be recovered without error, assuming the r_θ and r_ϕ surfaces are monotonic. The following analysis investigates the practical construction of the 2-D table with limited resolution and range that results in acceptable error. Later we will investigate cases where the r_θ and r_ϕ surfaces are not monotonic.

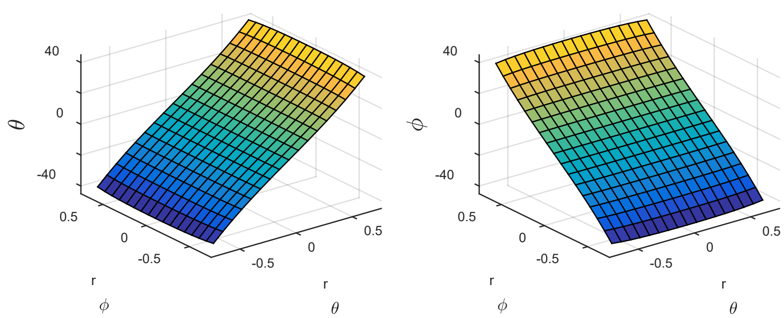

Fig. 8 2-D lookup tables for θ and ϕ

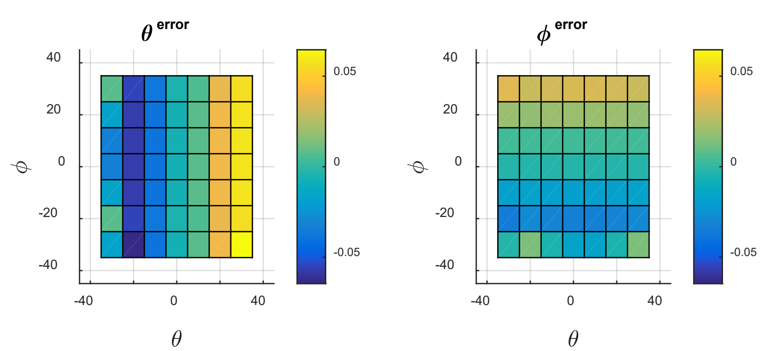

Fig. 9 Simulation results for θ and ϕ over the interval [45°,45°] using the lookup tables in Fig. 8. Excluded values occur outside the bounds of the lookup table.

When constructing the lookup table in Fig. 8, the minimum and maximum values of r_θ and r_ϕ for the given interval of θ and ϕ were used as the upper and lower bounds of the table. This resulted in some (r_θ, r_ϕ) points in the table outside of the r_θ and r_ϕ surfaces, leading to θ and ϕ lines with no intersections and, hence, the missing points in Fig. 9. In these cases, the lines can be extrapolated to determine an intersection point. The plot on the left in Fig. 10 shows lines that do not intersect. The plot on the right shows the lines extended through a spline interpolation, which results in an intersection point.

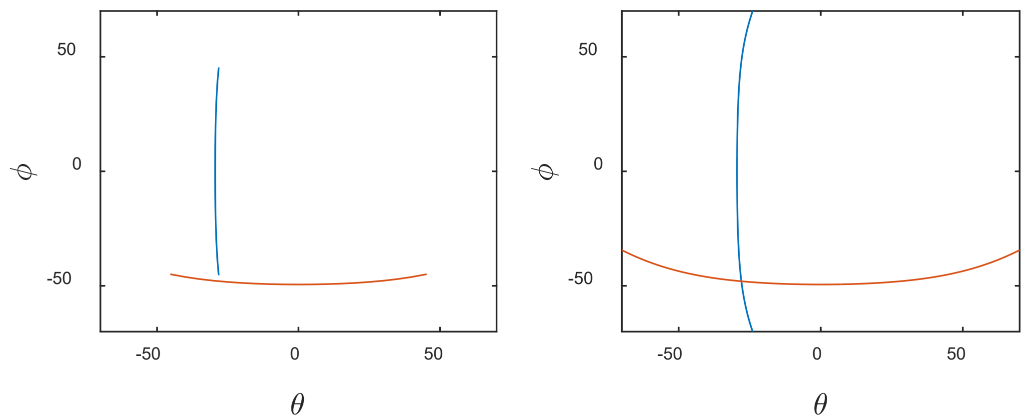

Fig. 10 Example of θ and ϕ curves that do not intersect to determine a (θ, ϕ) point (left), and the extended lines that do intersect (right)

Figure 11 shows the extended 2-D lookup table surfaces and error using spline interpolation. Although this interpolation method was successful in finding the missing values from Fig. 9, the values are not very accurate. The error plots show the greatest error around the edges where interpolation was used.

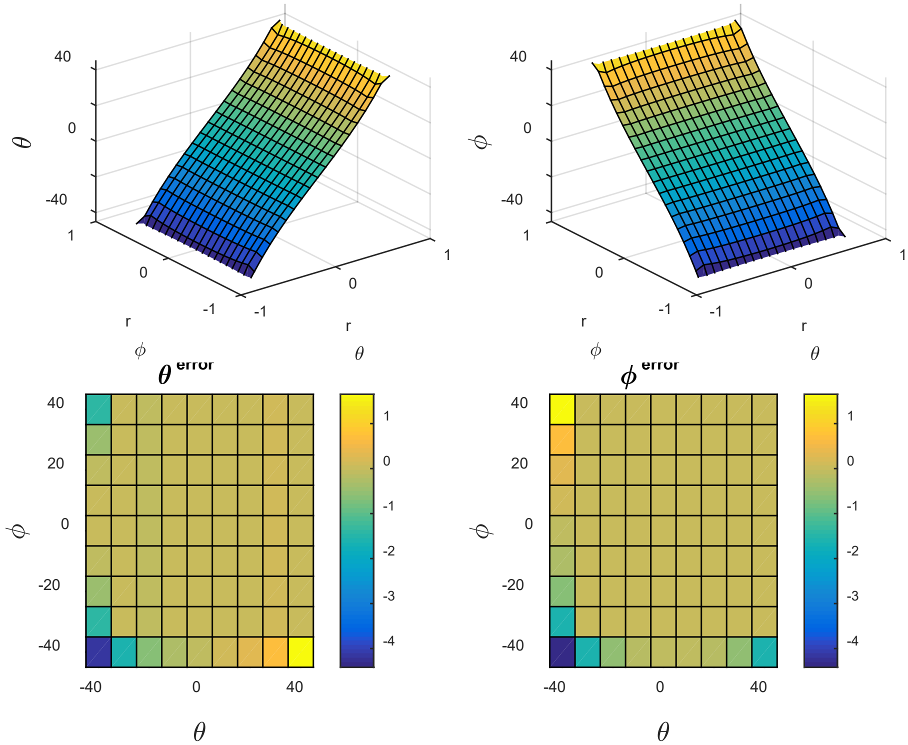

Fig. 11 Extended 2-D lookup tables using (top) interpolation of θ and ϕ curves and (bottom) the resulting error

To reduce this error, the tables can be extended to an interval greater than the interval used to measure error. This expands the original r_θ and r_ϕ surfaces, extending the θ and ϕ curves and increasing the number of (θ, ϕ) points that can be found without interpolation. The plot in Fig. 12 shows lookup tables constructed using a span of $[-55°, 55°]$ for θ and ϕ. The error plots can now span $[-45°, 45°]$ without extrapolation, resulting in lower error.

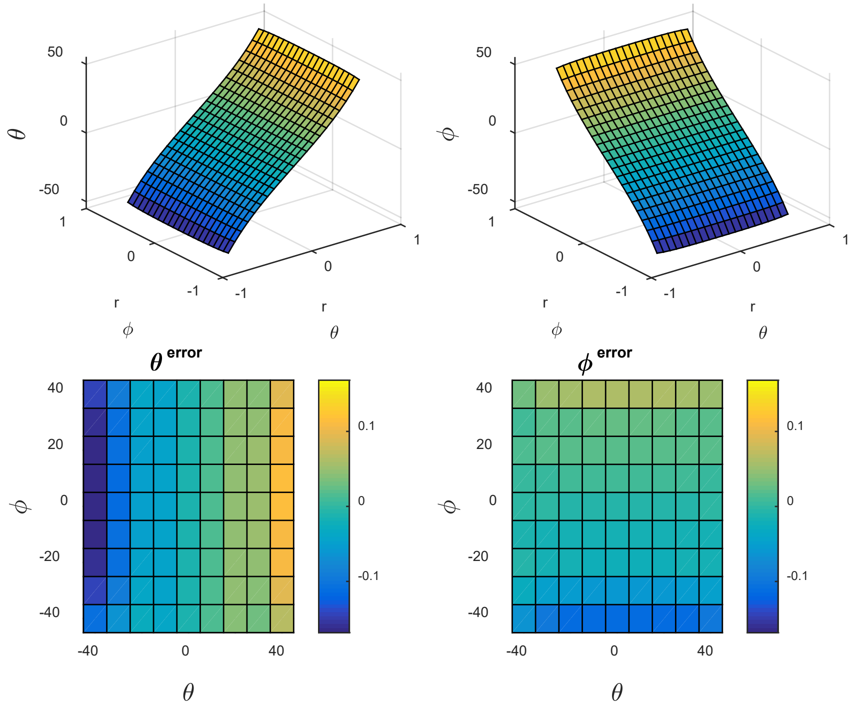

Fig. 12 2-D lookup tables using an extended range of $[-55°, 55°]$ for (top) θ and ϕ, and (bottom) the resulting error for θ and ϕ over a span of $[-45°, 45°]$

4.2 System Optimization

Now that an accurate 2-D lookup table has been constructed, it can be used to optimize a monopulse system over a range of parameters. The upper plots of Fig. 13 show (left) the minimum and (right) maximum error values for θ and ϕ in the interval $[-45°,45°]$. The bottom plots show the root mean squared error (RMSE) for (left) θ and (right) ϕ over a range of K and δ values. These plots show the antenna parameters that lead to stable models with low intrinsic errors. For this antenna model, there is a linear region centered approximately on $\delta = 18K + 0.8$ that leads to the highest performance. The missing data in the bottom two plots occur due to missing values in the lookup tables that occur for those values of K and δ even when the range of θ and ϕ expanded to the interval $[-55°, 55°]$.

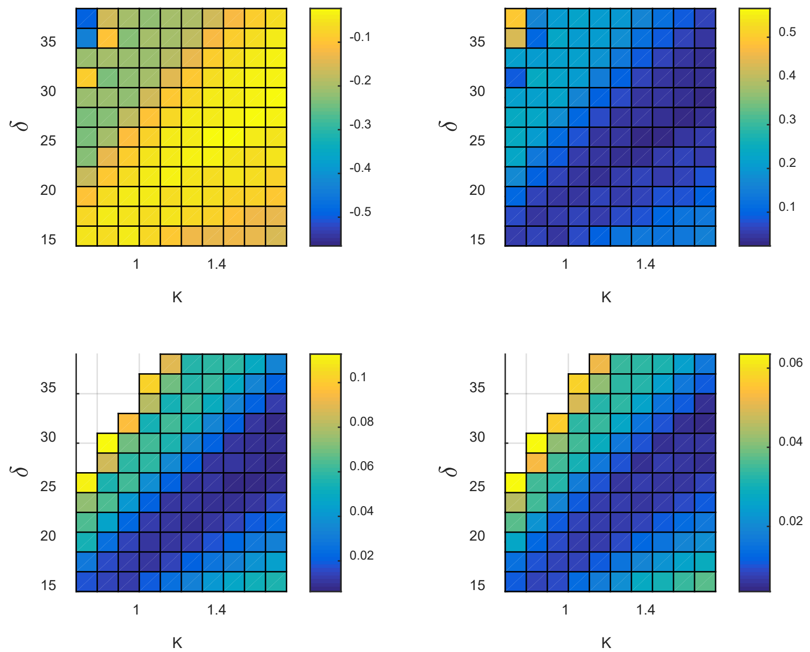

Fig. 13 Performance study over a range of antenna offsets (δ) and beamwidths (K). Upper plots show (left) the minimum and (right) maximum error values for θ and ϕ in the interval $[-45°, 45°]$ using a 2-D lookup table over a range of δ and K. Bottom plots show the RMSE error for (left) θ and (right) ϕ.

Additionally, the effect of additive noise can be modeled to determine the antenna pattern that is least sensitive to noise. Noise modeling also plays a role in system modeling, where the signal to noise ratio will depend on several parameters. Given an RF source with transmit power P_t, transmit antenna gain G_t, and the maximum gain of the monopulse antenna array G_r, the maximum received power is

$$P_r = P_t + G_t + G_r - FSPL, \tag{9}$$

where $FSPL$ is the free space path loss,

$$FSPL = 20\log_{10} d + 20\log_{10} f + 20\log_{10}\frac{4\pi}{c}, \tag{10}$$

with transmit frequency f, distance d, and speed of light c. The noise power is

$$P_n = kTB + NF, \tag{11}$$

where k is the Boltzmann constant, B is the bandwidth, T is the temperature, and NF is the system electronics noise figure.

Figure 14 shows the study in Fig. 13 repeated with additive noise based on the parameters in Table 2. Parameter N specifies the number of simulations repeated for each point. Therefore, the plots of the maximum error, minimum error, and RMSE now reflect the maximum error, minimum error, and RMSE over N

simulations. The optimal relationship between K and δ has shifted, with better performance for higher values of K.

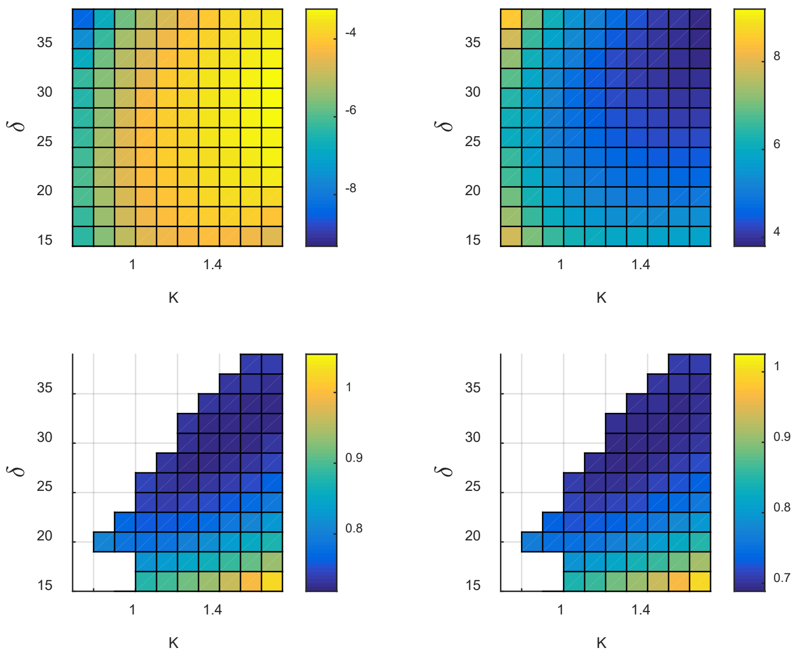

Fig. 14 Performance study over a range of antenna offsets (δ) and beamwidths (K) with noise. Upper plots show the (left) minimum and (right) maximum error values for θ and ϕ in the interval $[-45°, 45°]$ using a 2-D lookup table over a range of δ and K. Bottom plots show the RMSE error for (left) θ and (right) ϕ.

Table 2 Simulation parameters for study in Fig. 14

Parameter	Value
P_t	90 dBW
G_t	7 dBi
G_r	0 dBi
d	3000 m
f	10 GHz
P_n	–57 dBW
N	10

4.3 Alternative Antenna Model

The previous analysis used the Gaussian antenna model in Eq. 1. The system is fairly sensitive to the antenna pattern shape, motivating further analysis with other antenna patterns. An alternative antenna model[2] is given by

$$E(\theta, \phi) = \frac{\cos\left(K\pi\sqrt{(\theta-\delta_\theta)^2+(\phi-\delta_\phi)^2}\right)}{1-2K\sqrt{(\theta-\delta_\theta)^2+(\phi-\delta_\phi)^2}} + C, \tag{12}$$

where C is a constant to ensure that E is nonnegative. Using $\delta_\phi = \delta_\phi = 19°$ and $K = 1.3$, the four monopulse outputs are shown in Fig. 15. The top plots of Fig. 16 show the r_θ and r_ϕ surfaces over the interval $[-55°, 55°]$ for θ and ϕ. The bottom plots are side views of the top plots, showing r_θ and r_ϕ along a single angle. The top of Fig. 17 shows the 2-D lookup tables, with the resulting error for θ and ϕ on the bottom plots. Unlike the case of the Gaussian antenna models, there are unresolved points even though the range of the lookup tables were extended to an interval of $[-55°, 55°]$.

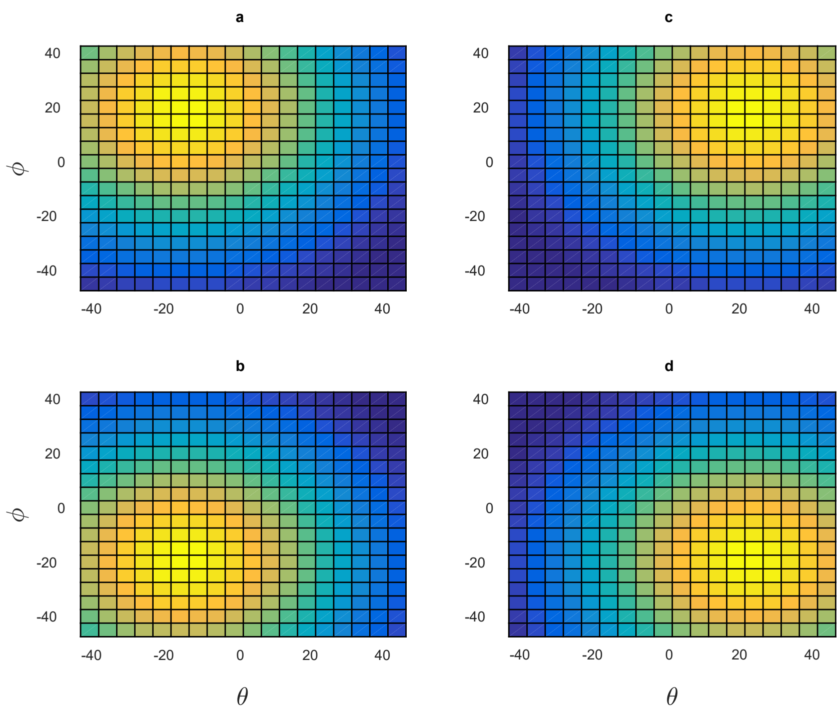

Fig. 15 Four-monopulse-element amplitudes using the alternative antenna model in Eq. 12

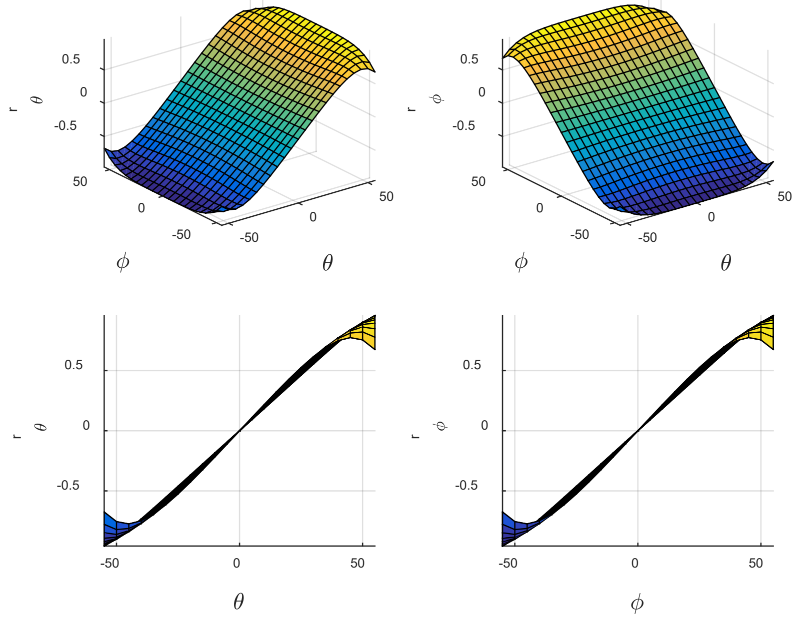

Fig. 16 r_θ and r_ϕ surfaces over the interval $[-55°, 55°]$ for (top) θ and ϕ and (bottom) side views showing r_θ vs. θ and r_ϕ vs. ϕ

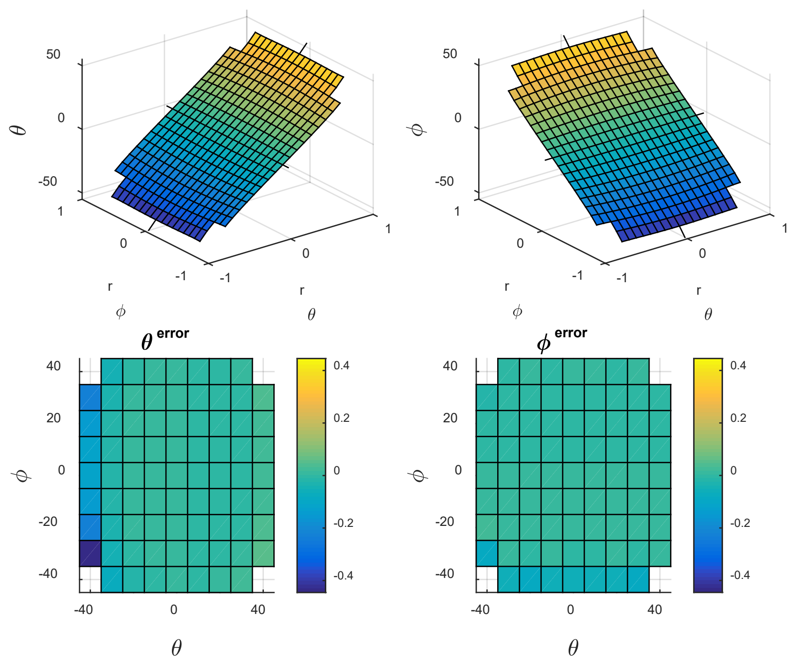

Fig. 17 2-D lookup tables using an extended range of $[-55°, 55°]$ for (top) θ and ϕ and (bottom) the resulting error for θ and ϕ over a span of $[-45°, 45°]$

In an attempt to solve this problem, the interpolation shown in Fig. 10 was used in conjunction with extending the range of the r_θ and r_ϕ surfaces, resulting in the 2-D lookup tables in Fig. 18. Unlike the Gaussian antenna model, interpolating the θ and ϕ curves did not succed in resolving all of the values in the tables. The reason for this is shown in Fig. 19: some of the curves contain multiple intersection points. As θ and ϕ increase, the r_θ and r_ϕ surfaces become more nonlinear, resulting in curves that may intersect more than once. For smaller values of θ and ϕ, the r_θ and r_ϕ surfaces are more linear, resulting in only one intersection. The following method was implemented to resolve multiple intersections. The lookup table was evaluated center out (i.e., from smaller values of θ and ϕ to larger values of θ and ϕ). Specifically, the evaluation order starts in the center at point $(0°, 0°)$ and spirals outward, as shown in Fig. 20. In the case of multiple intersection points, the point closest to the previous point is chosen. Figure 21 shows an example resolving θ and ϕ curves with multiple intersection points. The plots show the evaluation of two consecutive points. The plot on the left shows the point closer to the center, which is evaluated first. The plot on the right shows the evaluation of the next point, which is farther from the center, and contains multiple intersection points. The intersection point closest to the point on the left (circled) is chosen for the lookup table.

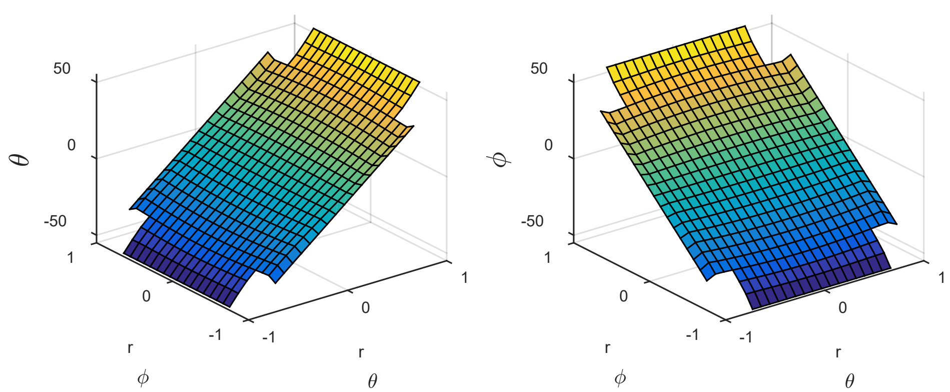

Fig. 18 2-D lookup tables using interpolation and an extended range of $[-55°, 55°]$ for θ and ϕ

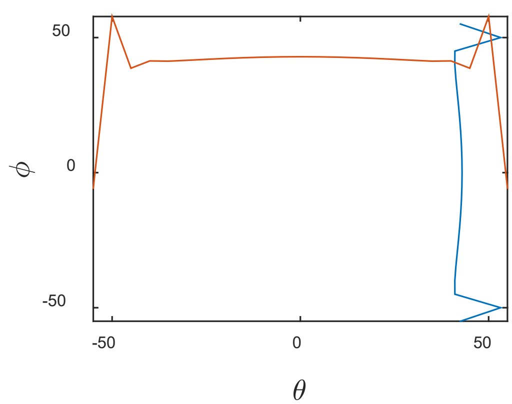

Fig. 19 Example θ and ϕ curves with multiple intersection points

43	44	45	46	47	48	49
42	21	22	23	24	25	26
41	20	7	8	9	10	27
40	19	6	1	2	11	28
39	18	5	4	3	12	29
38	17	16	15	14	13	30
37	36	35	34	33	32	31

Fig. 20 Example evaluation order of a 2-D table starting from the center and spiraling outward

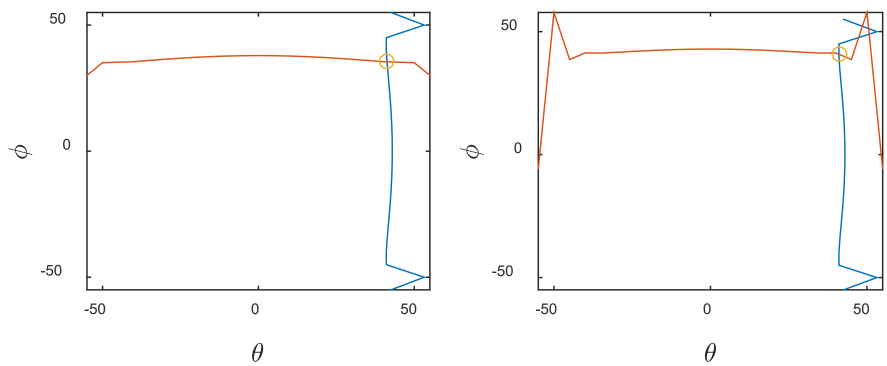

Fig. 21 Example resolving θ and ϕ curves with multiple intersection points. The multiple intersections on the right are resolved by choosing the point (circled) closest to the previous intersection point in the plot on the left.

Figure 22 shows lookup tables constructed using this new interpolation method. All of the points have now been resolved. Figure 23 shows the resulting error for θ and ϕ. Although the entire tables were resolved, the error is still much greater than the error shown in Fig. 12 for the Gaussian antenna model. Since the r_θ and r_ϕ surfaces become very nonlinear at large angles, extending the lookup tables too much can have a detrimental effect on performance. Figure 24 shows the error resulting from lookup tables that were only extended to $[-49°, 49°]$, which show a decrease in the maximum error. Finally, the table resolution can be increased from 5° steps to 2.5° steps, as shown in Fig. 25, which greatly reduces the error shown in Fig. 26. Now the performance of the lookup table for the alternative antenna model is equivalent to that of the Gaussian antenna model.

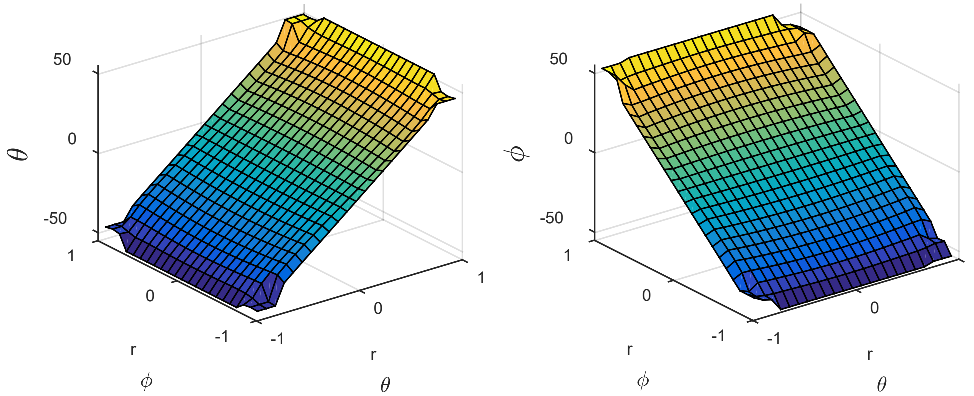

Fig. 22 2-D lookup tables using the new interpolation method and an extended range of $[-55°, 55°]$ for θ and ϕ

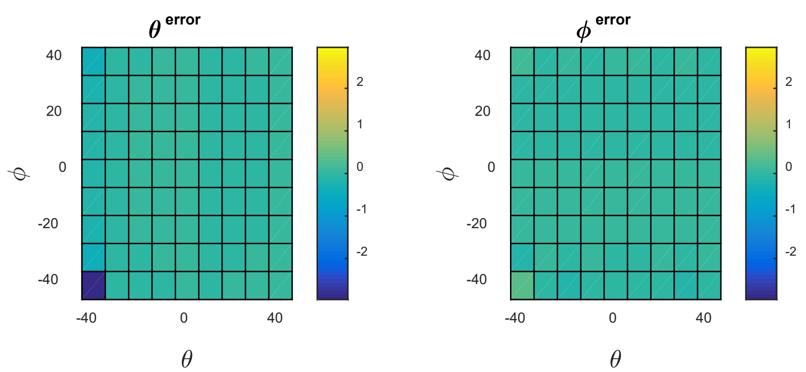

Fig. 23 Error for θ and ϕ over a span of $[-45°, 45°]$ using the lookup tables from Fig. 22

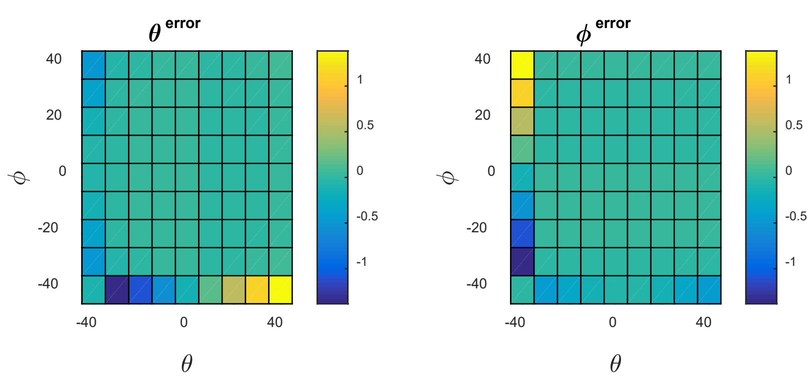

Fig. 24 Error for θ and ϕ over a span of $[-45°, 45°]$ using a lookup table from Fig. 22 over the reduced span of $[-49°, 49°]$

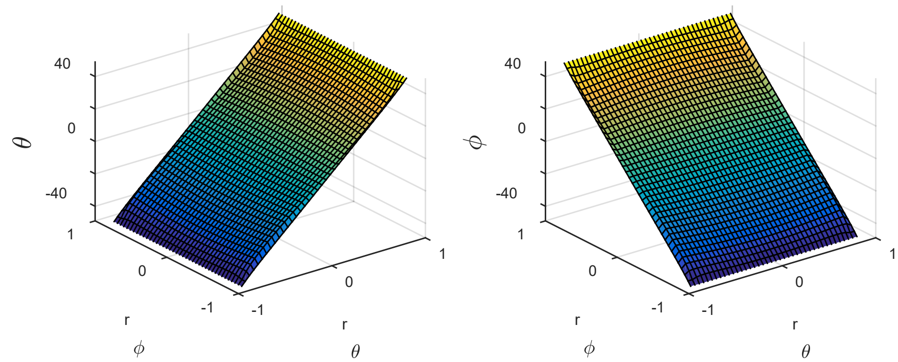

Fig. 25 2-D lookup tables using the new interpolation method and a range of $[-49°, 49°]$ with a resolution step size of $2.5°$ for $\boldsymbol{\theta}$ and $\boldsymbol{\phi}$

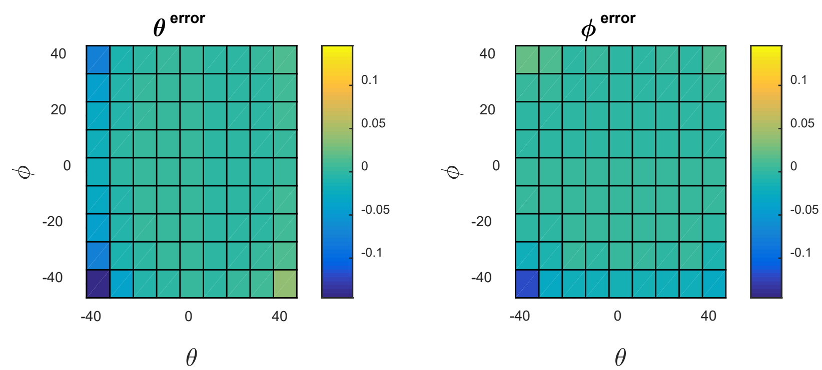

Fig. 26 Error for $\boldsymbol{\theta}$ and $\boldsymbol{\phi}$ over a span of $[-45°, 45°]$ using the lookup tables from Fig. 25

Using this lookup table for the alternative antenna model, the study in Fig. 13 was repeated. Figure 27 shows the results of this study, which are significantly different than the Gaussian antenna model study. Now, smaller values K appear to have better performance, while the regions of suitable δ values are relatively broad. Figure 28 shows the results of the study with noise, using the same parameters as before in Table 2. The results are similar to the noise-free case, except that the usable regions have narrowed slightly.

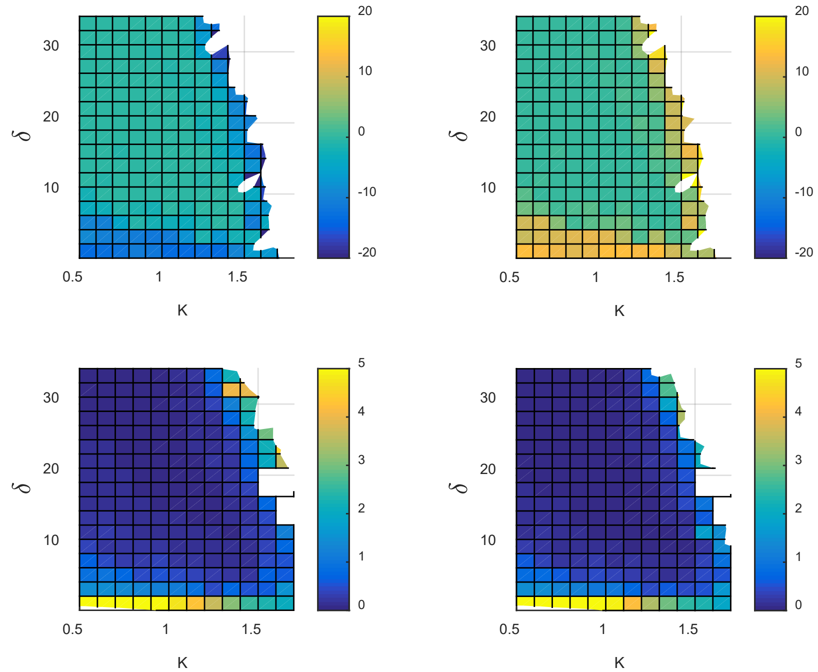

Fig. 27 Performance study over a range of antenna offsets (δ) and beamwidths (K) for the alternative antenna model. Upper plots show the (left) minimum and (right) maximum error values for θ and ϕ in the interval $[-45°, 45°]$ using a 2-D lookup table over a range of δ and K. Bottom plots show the RMSE error for (left) θ and (right) ϕ.

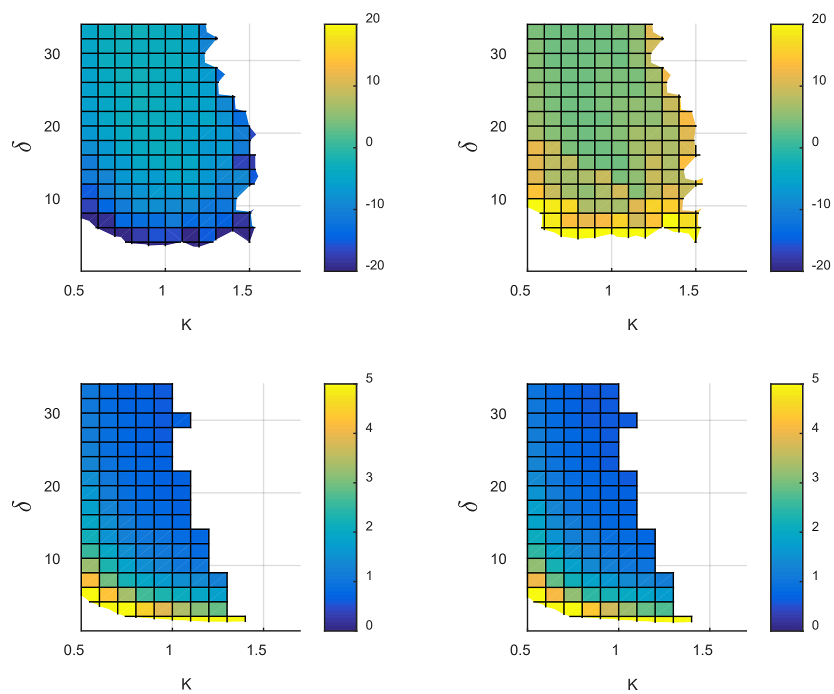

Fig. 28 Performance study over a range of antenna offsets (δ) and beamwidths (K) for the alternative antenna model with noise. Upper plots show the (left) minimum and (right) maximum error values for θ and ϕ in the interval $[-45°, 45°]$ using a 2-D lookup table over a range of δ and K. Bottom plots show the RMSE error for (left) θ and (right) ϕ.

4.4 RF Detector Model

Monopulse radar assumes invariance to scaling. Given scale factor s, dividing the Δ by Σ cancels out the scale factor as shown in Eqs. 13–17:

$$\Delta'_\theta = (sc+sd)-(sa+sb) = s\big((c+d)-(a+b)\big) = s\Delta_\theta. \tag{13}$$

$$\Delta'_\phi = (sa+sc)-(sb+sd) = s\big((a+c)-(b+d)\big) = s\Delta_\phi. \tag{14}$$

$$\Sigma' = sa+sb+sc+sd = s(a+b+c+d) = s\Sigma. \tag{15}$$

$$r'_\theta = \Delta'_\theta/\,\Sigma' = \ s\Delta_\theta/\,s\Sigma = \ \Delta_\theta/\,\Sigma = r_\theta. \tag{16}$$

$$r'_\phi = \Delta'_\phi/\Sigma' = s\Delta_\phi/s\Sigma = \Delta_\theta/\,\Sigma = r_\phi. \tag{17}$$

But the RF detection electronics that convert the RF power to a voltage level may be nonlinear. Figure 29 shows logarithmic and linear transfer characteristics of example nonlinear detector electronics.

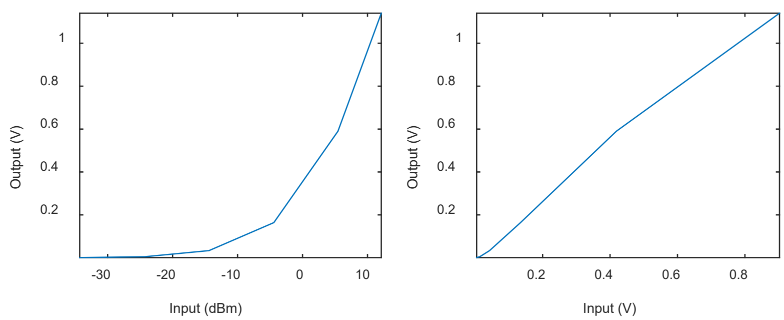

Fig. 29 (left) Logarithmic and (right) linear transfer characteristics of example RF detector electronics

If the detector is nonlinear, the scale factor s depends on amplitude, which in turn causes the monopulse ratio r to depend on amplitude. In this situation, how can a single 2-D lookup table relate the r values to the angles for all power levels? One method is to invert the detector model to remove this nonlinearity from the antenna outputs. Figure 30 shows the inverted models of the detector from Fig. 29. When constructing a lookup table from experimental data, an inverse transform can be used to determine the amplitude before the detector. In simulation, the 2-D lookup table can remain the same. Excluding the detector model is the same as modeling the detector and then removing it with an inverse model. When using the lookup table to convert r values to angles, the detector model is applied to the antenna amplitudes to simulate the measured signals. After measurement noise is added, the inverse detector model is used to estimate the signals before the detectors. These values are used to calculate the r values used in the lookup table. This process was implemented using the detector transfer characteristics shown in Fig. 29, and the trade studies in Fig. 27 and Fig. 28 were repeated. The results for the noise-free study are shown in Fig. 31, while Fig. 32 shows the simulation results using the parameters in Table 2 with noise. The results with the detector model are very close to those without the detector model, demonstrating that the inverse model was successfully used to remove effects of the RF detection electronics.

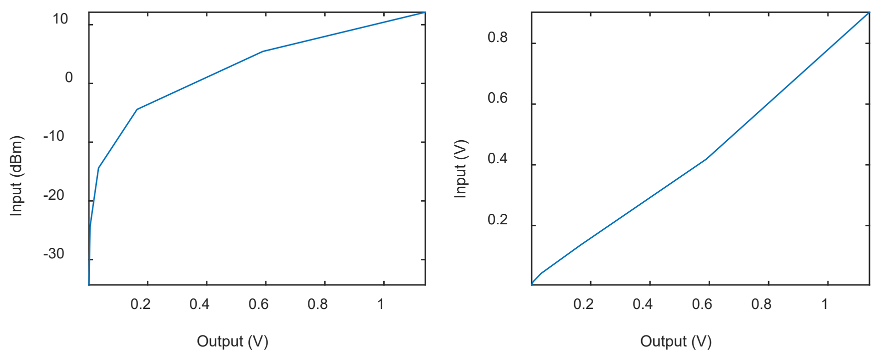

Fig. 30 Inverted transfer characteristics from Fig. 29

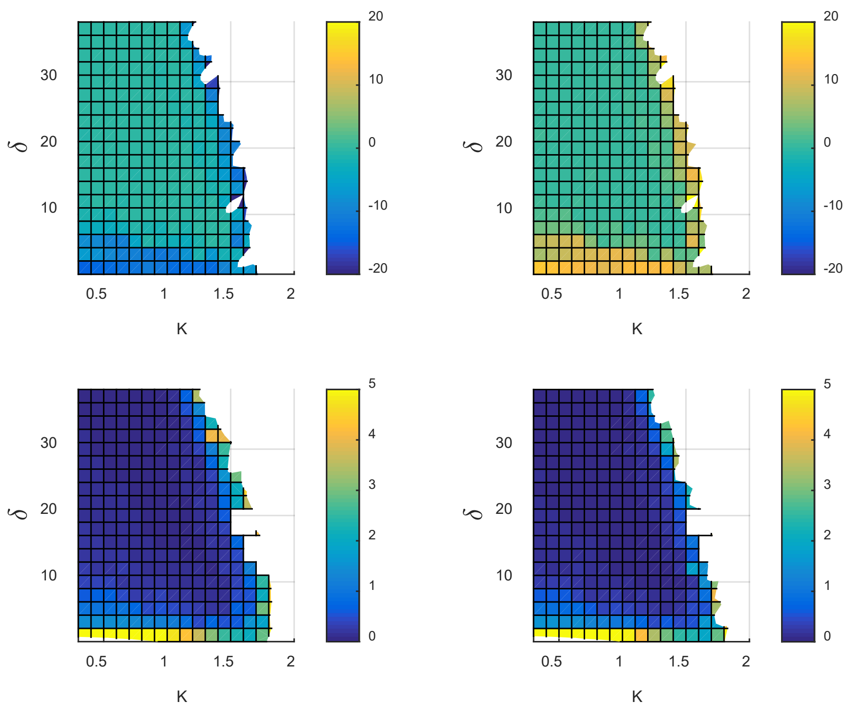

Fig. 31 Performance study over a range of antenna offsets (δ) and beamwidths (K) for the alternative antenna model with the RF detection included. Upper plots show (left) the minimum and (right) maximum error values for θ and ϕ in the interval $[-45°, 45°]$ using a 2-D lookup table over a range of δ and K. Bottom plots show the RMSE error for (left) θ and (right) ϕ.

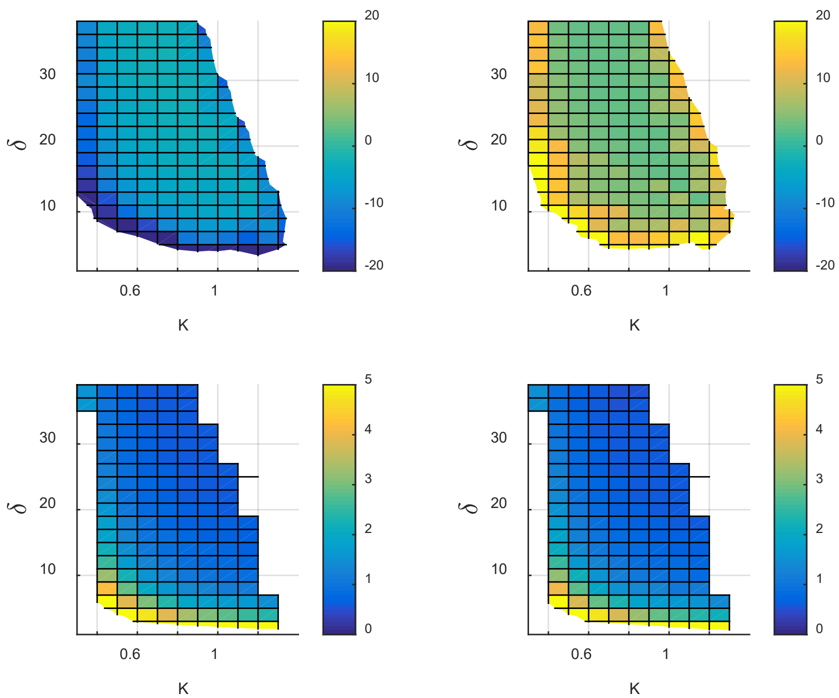

Fig. 32 Performance study over a range of antenna offsets (δ) and beamwidths (K) for the alternative antenna model with the RF detection included and added noise. Upper plots show the (left) minimum and (right) maximum error values for θ and ϕ in the interval $[-45°, 45°]$ using a 2-D lookup table over a range of δ and K. Bottom plots show the RMSE error for (left) θ and (right) ϕ.

5. Conclusion

This report has demonstrated the construction of a 2-D lookup table for monopulse radar. Linear models and 1-D lookup tables fail to capture the change in the r_θ and r_ϕ surfaces over ϕ and θ, respectively. 2-D lookup tables capture this effect, resulting in higher performance. The 2-D lookup table was evaluated with both a Gaussian antenna model and an alternative antenna model. Details such as the range of ϕ and θ used to evaluate the table, the table resolution, and the method used to resolve missing or multiple points all affect overall performance. Modeling is completed with the addition of noise and RF detection modeling, allowing for the optimization of system parameters through trade studies.

6. References

1. Barton DK, editor. Monopulse radar. In: Radars. Vol. 1. Norwood (MA): Artech House; 1977.
2. Sherman SM, Barton DK. Monopulse principles and techniques. 2nd ed. Norwood (MA): Artech House; 2011.
3. Cole EL Jr, Enstrom RA, Olver TE, inventors. Northrop Grumman Corp., assignee. Secondary radar digital monopulse receiving apparatus and method. United States patent US 5,619,206. 1997 Apr 8.
4. Adams NH, Sequeira HB, Bray M, Srinivasan D, Schulze R, Berman S, Ambrose H. Monopulse autotrack methods using software-defined radios. Proceedings of the IEEE Aerospace Conference; 2015 Mar. p. 1–6.
5. Goldsmith PF. Radiation patterns of circular apertures with Gaussian illumination. Int J Infr Mill Waves. 1987;8.7:771–781.
6. Skolnik MI. Radar handbook. New York (NY): McGraw-Hill Education; 1970.

List of Symbols, Abbreviations, and Acronyms

1-D	1-dimensional
2-D	2-dimensional
DOA	direction of arrival
RF	radio frequency
RMSE	root mean squared error

1 (PDF)	DEFENSE TECHNICAL INFORMATION CTR DTIC OCA
1 (PDF)	CCDC ARL FCDD RLD CL TECH LIB
27 (PDF)	CCDC ARL FCDD RLW LF B ALLIK B J ACKER T G BROWN S BUGGS E BUKOWSKI J COLLINS J CONDON B DAVIS M DON D EVERSON R HALL J HALLAMEYER M HAMAOUI T HARKINS M ILG B KLINE J MALEY C I MILLER B NELSON D PETRICK K PUGH N SCHOMER B TOPPER FCDD RLS RM M GOVONI T K ANTHONY J T CLARK FCDD RLW C C KRONINGER